Contents lists available at ScienceDirect

Chemical Engineering Research and Design

journal homepage: www.elsevier.com/locate/cherd

Effect of the reduction degree of graphene oxide on the adsorption of Bisphenol A

Sotiria Bele[a], *Victoria Samanidou*[b], *Eleni Deliyanni*[a,*]

[a] *Division of Chemical Technology, Department of Chemistry, Aristotle University of Thessaloniki, GR-541 24 Thessaloniki, Greece*

[b] *Laboratory of Analytical Chemistry, Department of Chemistry, Aristotle University of Thessaloniki, GR-541 24 Thessaloniki, Greece*

ARTICLE INFO

Article history:
Received 21 December 2015
Received in revised form 24 February 2016
Accepted 3 March 2016
Available online 9 March 2016

Keywords:
Graphite oxide
Graphene
Bisphenol A
Adsorption
Kinetics

ABSTRACT

Graphite oxide (GO) was reduced to different reduction degrees by using hydrazine hydrate and finally to graphene using NH_4OH. The obtained materials were characterized by X-ray diffraction (XRD), scanning electron microscopy (SEM), nitrogen adsorption (BET), Fourier transform infrared spectroscopy (FTIR) and potentiometric titration measurements. Their adsorption performance for Bisphenol A (BPA) was evaluated taking into account pH, ionic strength, kinetics initial ion concentration and thermodynamics of adsorption. The adsorption capacities were increased with increasing the reduction degree of GO with the maximum adsorption capacity (Q_{max} = 94.06 mg/g) to be presented by Graphene that was the result of the optimum reduction degree. The adsorption followed pseudo-second order kinetics and the thermodynamic analysis indicated that it was spontaneous and endothermic. The increase in the degree of GO reduction reduced the amount of oxygen-containing functional groups on the surface of reduced samples, resulting to the increase of the π–π interaction between sorbent–adsorbate and to linear increase of adsorption capacity.

1. Introduction

Endocrine-disrupting chemicals (EDCs) can imitate the biological activity of natural hormones, occupy the hormone receptors, or interfere with the transport and metabolic processes of natural hormones, finally pose a risk to animals and humans (Ternes et al., 1999; Chang et al., 2009). Hence, EDCs have drawn considerable social and scientific concern in recent years. Bisphenol A (BPA), one of these EDCs, is widely used as a monomer for the production of epoxy resins, polycarbonates, and other plastics. It is considered to be a critical contaminant because its weak estrogen-like effect is harmful to organisms (Furhacker et al., 2000; Kang et al., 2006; Staples et al., 1998). BPA contamination has been reportedly detected in industrial wastewater, groundwater, surface water, and even drinking water (Staples et al., 2000; Lee and Peart, 2000; Belfroid et al., 2002). Therefore, BPA is selected as the model compound for the removal of water among the EDCs herein. Nowadays, various removal methods have been used in water treatment, such as adsorption (Pan et al., 2009; Dong et al., 2010; Liu et al., 2009; Kim et al., 2011), membrane separation (Zhang et al., 2006), biological treatment (El-Naas et al., 2009), photocatalytic degradation (Ahmaruzzaman, 2008) and other processes. Among these methods, adsorption is a superior and widely used method in terms of its comparatively low cost, ease of operation, and fewer harmful secondary products. Regarding the adsorption technique, the application of effective adsorbents is critical to guaranteeing the efficiency of water treatment (Harikishore Kumar Reddy and Lee, 2013; Wang et al., 2009).

Carbonaceous materials such as activated carbon (AC) (Liu et al., 2009; Bautista-Toledo et al., 2005) carbon nanotubes

* *Corresponding author.* Tel.: +30 2310 997808; fax: +30 2310 997859.
E-mail address: lenadj@chem.auth.gr (E. Deliyanni).
http://dx.doi.org/10.1016/j.cherd.2016.03.002

(CNTs) (Kuo, 2009), porous carbon (Asada et al., 2004) and graphene oxide (Gao et al., 2012; Zhang et al., 2011a,b,c) have always attracted attention because of their chemical stability, large specific surface area, abundant pore size distribution, and feasibility of mass production. Thus, it is important to seek new carbonaceous adsorbents with a high adsorption capacity, fast adsorption rate and specific surface reactivity.

Graphite oxide (GO), an oxygen-rich derivative of graphite, has been extensively investigated in recent years. It exhibits an extended layered structure with plenty of hydrophilic oxygen containing groups (—OH, —COOH, —CHO, and epoxy groups) on the graphitic backbone (Dikin et al., 2007). Additionally, GO can be obtained from cheap natural graphite in large quantities, and shows excellent adsorption capacity for the removal of heavy metal ions (Fan et al., 2012; Yang et al., 2010), dyes (Zhang et al., 2011a,b,c) and antibiotics (Gao et al., 2012) from aqueous solutions.

It is known that the surface of GO has different oxygen-containing functional groups. These functional groups determine the charge, hydrophobicity, electron density of the layers and alter the interaction between phenolic compounds and GO through π–electron donor–acceptor (π–EDA) bonds, and hydrogen bonds (Shniepp et al., 2006; Mkhohan et al., 2009). The structure and properties of phenolic compounds such as aromatic ring substitution, solubility, and pKa may influence the affinity between phenolic compounds and GO. The solution pH also affected the adsorption of phenolic compounds. The reduction of GO will change the amounts and distributions of oxygen-containing functional groups on its surface. It is important to find the correlation between the adsorption ability and reduction degree of GO, which will guide the tuning of the adsorption of organic pollutants (such as phenolic) on reduced graphene oxide (RGO). The use of hydrazine easily yields a high degree of reduction of GO.

Graphene (Gr), a single atomic layer of sp2-hybridized carbon arranged in a honeycomb structure, is the 2D allotrope of carbon. It has drawn enormous scientific attention since its discovery because of its large surface area (Lee et al., 2008), extraordinary electronic and mechanical properties, excellent mobility of charge carriers, and good thermal conductivity (Balandin et al., 2008). Owing to these remarkable properties, graphene is likely to be applied in many fields such as supercapacitors, solar cells, sensors, and adsorbents (Stoller et al., 2008; Wang et al., 2008). Recently, it has been reported that graphene shows excellent adsorption capacity for the removal of heavy metal ions (Pb(II), Cd(II), Cr(VI), etc.), fluoride ions (Wang et al., 2008), and dyes (methyl orange, methyl blue, rhodamine B, etc.) from aqueous solutions (Li et al., 2011). Compared to other carbonaceous materials, the advantage of graphene is the selective adsorption ability to those aromatic compounds with benzene rings through strong π−π interaction. Therefore, graphene is expected to be a promising adsorbent for the removal of aromatic compounds in water treatment.

In the current study, the removal behavior of BPA from water by GO, RGO and Gr as a function of solution characteristics, including BPA concentration, pH, ionic strength, and temperature, was investigated systematically. Our main purpose was to reveal the effects of reduction degree of GO on the adsorption of BPA and then to clarify the possible adsorption mechanisms of this endocrine disruptor on GO, RGO and Gr. The adsorption capacity was evaluated and adsorption mechanism of BPA by GO, RGO and Gr was proposed.

2. Materials and methods

2.1. Chemical reagents

Graphite, Bisphenol A, sulfuric acid, $KMnO_4$ and hydrogen peroxide were purchased from Sigma Aldrich (St. Louis, MO, USA). Acetonitrile HPLC gradient grade was supplied by Chem-Lab (Chem-Lab NV, Zedelgem, Belgium). All the reagents were analytical grade (puriss. pa. ≥ 98.5%).

2.2. Preparation of graphite oxide

Graphite oxide was prepared by a modified Hummers method (Hummers and Offeman, 1958). Graphite (10 g) was mixed with 230 mL of H_2SO_4 (98% (*w*)) in a 500 mL flask in an ice bath. After 30 min of stirring, $KMnO_4$ (30 g) was added dropwise into the vigorously stirred suspension below 20 °C until it gradually became a brownish slurry, and then was diluted slowly with 230 mL of water and further, 1400 mL of water and 100 mL of H_2O_2 (30% (*w*)) were added. For purification, the mixture was centrifuged and washed with 10% HCl and then deionized water several times to remove the residual metal ions and acid. After filtration and freeze–drying GO was obtained as powder.

2.3. Synthesis of reduced graphite oxide (RGO)

A given amount of GO was dispersed into 100 mL of water, into which aqueous hydrazine hydrate solution (80 wt.%) were added. The reduction of GO was carried out under stirring at 95 °C for 5 h. The solids were isolated by filtering with 0.22 μm filter and washed with distilled water in order to remove the excess hydrazine. Finally, the product was freeze-dried (Stankovick et al., 2007). The mass ratio of hydrazine hydrate to GO was controlled at 0.5:1, 1:1 and 2:1 in order reduced graphite oxide at different reduction degree to be prepared, $RGO_{0.5:1}$, $RGO_{1:1}$ and $RGO_{2:1}$, respectively. When it is not otherwise mentioned, RGO is for $RGO_{1:1}$. This sample was further sonicated and was designated as RGOs.

2.4. Synthesis of graphene

Graphene was synthesized after the hydrazine reduction of GO. A 250 mL GO aqueous dispersion (2 mg/mL) was ultra sonicated for 2 h. The solution pH was adjusted to 10 by adding 30% ammonia solution. Then, 5 mL of hydrazine hydrate (80 wt.%) was added to the solution at 95 °C and stirred for 5 h. The black solution was filtered, washed thoroughly with deionized water in order to remove the excess hydrazine. Finally, the product was freeze-dried and graphene was obtained that was designated as Gr (Meyer et al., 2007).

2.5. Characterization—Instrumentation

Scanning electron microscopy (SEM) images were performed with electron microscope (model Zeiss Supra 55 VP, Jena, Germany) and the accelerating voltage was 15.00 kV.

Nitrogen isotherms were measured using AS1Win (Quantachrome Instruments, FL, USA) at liquid N_2 temperature (77 K). The samples were degassed at 150 °C in a vacuum system at 10^{-4} Torr before the analysis. The specific surface area (S_{BET}) was calculated from the isotherm data using the Brunauer, Emmet and Teller (BET) model and the pore size distribution curves were obtained using density functional theory (DFT)

method. The total pore volumes (V_{tot}) were obtained from the volumes of nitrogen adsorbed at a relative pressure of 0.99 cm^3/g.

FTIR spectra of the samples were taken with a Nicolet 560 (Thermo Fisher Scientific Inc., MA, USA) FTIR spectrometer. The spectra were recorded in transmission mode using potassium bromate wafers containing 0.5 wt.% of carbon. Pellets made of pure potassium bromate were used as the reference sample for background measurements. The spectra were recorded from 4000 to 400 cm^{-1} at a resolution of 4 cm^{-1} and are baseline corrected.

Potentiometric titration measurements were carried out with a T50 automatic titrator (Mettler Toledo, Columbia, USA). 0.1 g of carbon were placed in 50 mL of $NaNO_3$ solution (0.01 mol/L) as supporting electrolyte and stirred overnight. The solution was titrated with NaOH (0.1 mol/L) under N_2 saturation. The titrations were carried out over a wide range of pH. The total surface charge, Q_{surf} (mmol/g), was calculated as a function of pH by the following equation (Triantafyllidis and Deliyanni, 2014):

$$Q_{surf} = \frac{C_A + C_B + [H^+] + [OH^-]}{W} \quad (1)$$

where C_A and C_B (mol/L) are the acid and base concentrations, respectively; $[H^+]$ and $[OH^-]$ are the equilibrium concentrations of those ions (mol/L), and W (g/L) is the solid concentration.

After adsorption, the suspensions were centrifuged and the supernatant solution was filtered through a 0.22 μm membrane. The concentration of the remaining in the solution BPA was examined by a high-performance liquid chromatography HPLC). The separation of the monomers was performed using a HPLC column 250 × 4.6 mm (PerfectSil Target ODS-3 5 μm, MZ-Analysentechnik GmbH, Mainz, Germany) with a mobile phase consisted of mixture of water and acetonitrile (70%CH_3CN/30%H_2O), delivered isocratically. The pressure observed was 100 bar at a flow rate of 1.0 mL/min. Bisphenol A was identified by comparison of its retention time with that of the reference compounds under the same HPLC conditions. A Shimadzu (Kyoto, Japan) LC-10AD pump was used to deliver the mobile phase to the analytical column. Sample injection was performed via a Rheodyne 7125 injection valve (Rheodyne, Cotati CA, USA) with a 20 μL loop. Detection was achieved by an SSI 500 UV–vis detector (SSI, State College, PA, USA) at a wavelength of 230 nm and a sensitivity setting of 0.002 AUFS.

2.6. Adsorption experiments

2.6.1. Effect of pH on adsorption

The effect of pH was conducted by mixing 0.05 g of adsorbent with 20 mL (V) of BPA solution (C_0 = 60 mg/L) in capped vials. The pH value, ranging between 2 and 6, was kept constant throughout the adsorption process by micro-additions of HNO_3 (0.01 mol/L) or NaOH (0.01 mol/L). The suspensions were shaken for 24 h (agitation rate: N = 140 rpm) into a water bath to control the temperature at 25 °C. The optimum pH (for performing the equilibrium experiments) was found to be 3.

2.6.2. Effect of ionic strength on adsorption

The effect of ionic strength on the adsorption of BPA by GO, RGO and Graphene were examined by mixing 0.05 g of adsorbent with 20 mL (V) of BPA solution (C_0 = 60 mg/L) in capped vials. The NaCl concentrations ranged between 0.01 and 1 M. The suspensions were shaken for 24 h (agitation rate: N = 160 rpm) into a water bath to control the temperature at 25 °C at pH = 3.

2.6.3. Effect of contact time

Kinetic experiments were performed by dispersing 0.05 g of adsorbent in 20 mL (V) of BPA solution (C_0 = 60 mg/L) in capped vials. The suspensions were shaken for 24 h at optimum pH = 3 in water bath at 25 °C (N = 160 rpm) for different times (5 min–24 h). The experimental kinetic data were fitted to pseudo-first [Eq. (2)] and pseudo-second order kinetic models that are [Eq. (3)] the most widely-used kinetic models in adsorption works. The linearized-integral form of the pseudo-first-order model is given by the following equation (Blanchard et al., 1984):

$$\ln(q_e - q_t) = \ln q_e - k_1 t \quad (2)$$

where q_e and q_t are the amounts of BPA adsorbed at equilibrium and at time t (mg/g), respectively, and k_1 is the Lagergren rate constant of adsorption (min^{-1}). The values of q_e and k_1 can be found from the intercept and slope of the linear plot of $\ln(q_e - q_t)$ versus t.

The pseudo-second-order model includes all the steps of adsorption including external film diffusion, adsorption, and internal particle diffusion. The linearized-integral form of the pseudo-second order model is

$$\frac{t}{q_t} = \frac{1}{K_2 q_e^2} + \frac{t}{q_e} \quad (3)$$

where k_2 is the pseudo-second order rate constant of adsorption (g/mg min) (Ho, 2006; Sparks, 1986). The slope and intercept of the linear plot of t/qt against t yield the values of q_e and k_2. Furthermore, the initial adsorption rate h (mg/g/min) can be estimated from the equation:

$$h = K_2 q_e^2 \quad (4)$$

2.6.4. Effect of initial ion concentration—Isotherms

The effect of initial ion concentration on equilibrium was examined by mixing 1 g/L of adsorbents with 20 mL of ion solutions of varying initial concentrations (C_0 = 10–500 mg/L). The suspensions were shaken overnight at pH = 3 in water bath at 25 °C (N = 160 rpm).

The experimental equilibrium data were fitted to the Freundlich (1906) [Eq. (5)] and Langmuir (1918) [Eq. (6)] isotherms expressed by the following equations:

$$Q_e = K_F C_e^{1/n} \quad (5)$$

$$Q_e = \frac{Q_m K_L C_e}{1 + K_L C_e} \quad (6)$$

where Q_m (mg/g) is the maximum adsorption capacity; K_L (L/mg) is the Langmuir adsorption equilibrium constant; K_F ($mg^{1-1/n} L^{1/n}/g$) is the Freundlich constant representing the adsorption capacity; n (dimensionless) is the constant depicting the adsorption intensity.

The equilibrium amount in the solid phase (Q_e, mg/g) was calculated according to the following equation:

$$Q_e = \frac{(C_0 - C_e)\,V}{m} \quad (7)$$

2.6.5. *Effect of temperature—Thermodynamics*

To study the effect of temperature on equilibrium, the same experiments as those for the study of the effect of initial ion concentration on equilibrium were performed, but at different temperatures (25, 45, and 65 °C), in order to investigate the thermodynamic behavior of the sorbents-BPA system. For this purpose, the change of Gibbs free energy (ΔG°, kJ/mol), enthalpy (ΔH°, kJ/mol) and entropy (ΔS°, kJ/mol K)) were calculated, based on the isotherms at 25, 45, and 65 °C. The equations below were used for the calculation of the aforementioned thermodynamic parameters (where C_s (mg/L) is the amount adsorbed on a solid at equilibrium and R (8.314 J/mol/K) is the universal gas constant) (Foo and Hameed, 2012):

$$K_c = \frac{C_s}{C_e} \tag{8}$$

$$\Delta G^\circ = RT \ln (K_c) \tag{9}$$

$$\Delta G^\circ = \Delta H^\circ - T\Delta S^\circ \tag{10}$$

$$\ln (K_c) = \left(-\frac{\Delta H^\circ}{R}\right)\frac{1}{T} + \frac{\Delta S^\circ}{R} \tag{11}$$

where ΔG° was given from Eq. (9), while ΔH° and ΔS° were given from the slop and intercept of the chart between $\ln(K_c)$ versus $1/T$ (Eq. (11)).

2.6.6. *Desorption*

Desorption experiments were carried out by mixing in flasks the amount of BPA-loaded sorbents, after adsorption, with 20 mL of deionized water (same amount of sorbent and same volume as in the adsorption procedure) over a pH range between 3 and 11, at 25 °C for 24 h (agitation rate = 160 rpm). The desorption percentage was calculated from the difference between the loaded amount of BPA on adsorbent after adsorption and the amount of BPA in solution after desorption. This procedure was made to determine the optimum desorption pH value of the BPA-loaded graphite materias. Besides, organic solvents were also tested as eluents. The organic solvents were: diethyl ether-methanol 9:1 v/v, ethanol, acetonitrile and methanol. The collected, after adsorption, amount of BPA-loaded sorbents were mixed in flasks, with the same amount of sorbent and same volume as in the adsorption step and after 24 h (agitation rate = 160 rpm), the supernatants were collected, filtered through 22 μm pore size membrane and measured for the remaining BPA concentrations. This procedure was made to determine the organic solvent that could eluent the greater amount of BPA from the BPA-loaded sorbents.

3. Results and discussion

3.1. *Effect of pH*

The pH of the solution plays an important role on the adsorption because it influences both the surface charging of the adsorbent and the dissociation state of the adsorbate related to their dissociation constants (pKa). Fig. 1a presents the effect of the solution pH on BPA adsorption by GO, RGO and Gr, for initial pH range 3.0 to 10.0.

With the pH increase, the adsorption capacity of GO decreased, with the maximum uptake to be at pH 3.0 and the per cent removal to decrease from 85% at pH 3.0 to 50% at pH

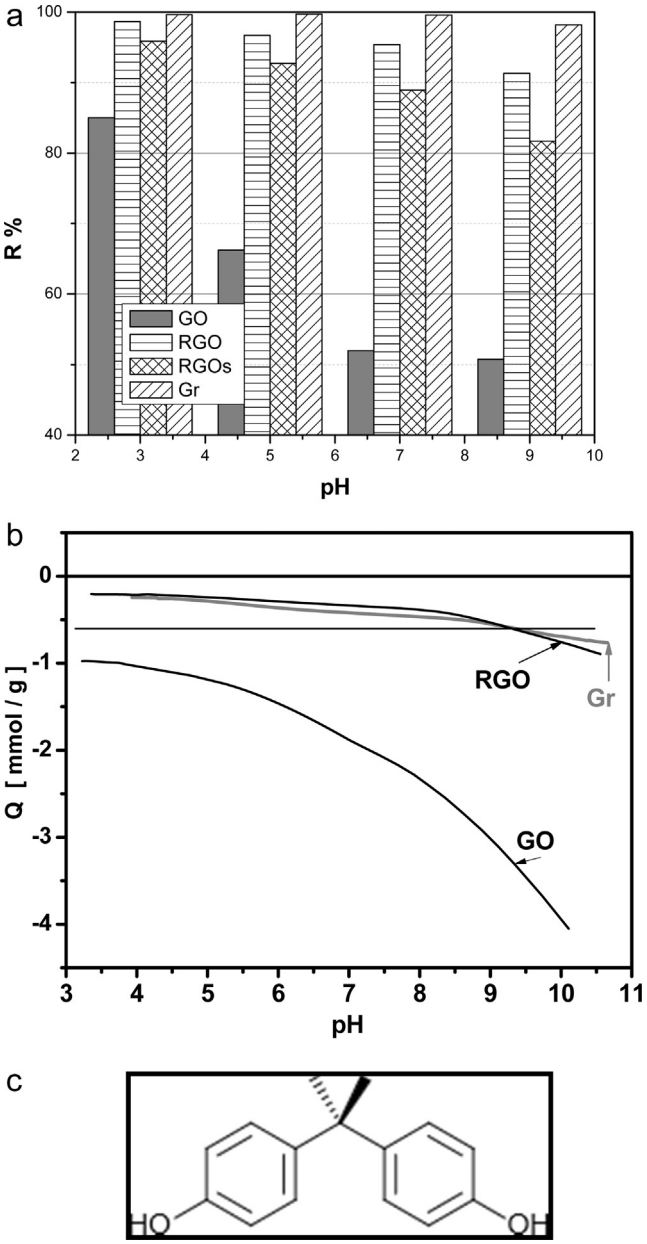

Fig. 1 – (a) Effect of pH on BPA adsorption onto GO, RGO, RGOs and Gr. (b) Potentiometric titration results for GO, RGO and Gr. (c) Bisphenol A, BPA.

9.0. Bisphenol A (Fig. 1c) has a value of pKa = 10.6 (Bautista-Toledo et al., 2014). In aqueous solutions BPA is present in its molecular form for pH < ~9 while for pH values 8–12 it is present as $HBPA^-$ or (for pH values >9) as BPA^{2-} as was referred from the species distribution diagram for BPA (Bautista-Toledo et al., 2005, 2014). It is seen that the effect of pH on BPA sorption on GO is well correlated to the net surface charge of GO at different pH values and the surface charge of BPA species. GO was negatively charged over the whole pH range, as presented in the relative proton-binding curve from the potentiometric titration results (Fig. 1b), due to the abundance of oxygen-containing surface functional groups. Since at high pH values, these functional groups were deprotonated to form negative surface charges, the electrostatic repulsions decreased the adsorption ability of GO for the negatively charged BPA molecules at this pH range.

There are two factors influencing the adsorption of BPA, hydrogen-bond interaction between the hydroxyl groups of

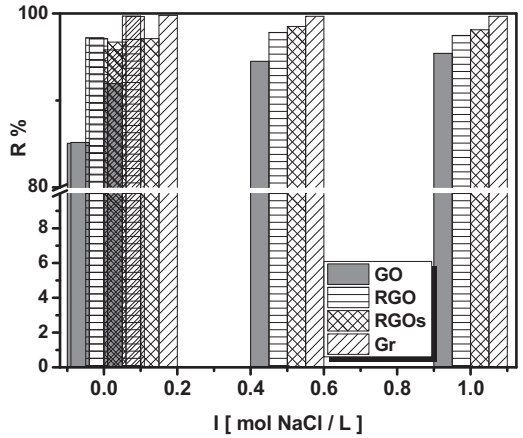

Fig. 2 – Effect of ionic strength on BPA adsorption onto GO, RGO, RGOs and Gr.

adsorbent and BPA and π–π interactions (Xuebao, 2013). π–π interactions are developed between the benzene-ring of BPA and the skeleton of the sorbents, since BPA contained electrons which could interact with the electrons of the graphene based sorbents. As also presented in Fig. 1a, the R% values for both RGO and Gr showed little change with increasing pH up to pH = pKa of BPA, due to their less oxygen polar groups compared to GO, as it also presented in Fig. 1b, that results at reduced electrostatic repulsions between BFA and the less negatively charged surface of these adsorbents. In such cases, BPA can be adsorbed on the sorbent surface by π–π electron and hydrophobic interaction (Bautista-Toledo et al., 2014). RGO and Gr as it is seen from Fig. 1a could be efficient adsorbents for the removal of organic molecules over a wide pH range (Wang and Chen, 2015). Since the maximum adsorption was attained at pH of 3.0 for all samples, as in the case of GO, for this reason equilibrium experiments were performed at the pH = 3 for all sorbents.

3.2. *Effect of ionic strength*

Industrial sewage contains high concentrations of salts, which may affect the removal of pollutants. Thus, the effect of the solution ionic strength on the adsorption of BPA by GO, RGO and Gr was examined. The adsorption capacity was found to increase slightly with the increase of NaCl concentration (more than 0.1 mol/L). This may be attributed to the salting out effect of electrolytes via decreasing the solubility of BPA and enhancing its adsorption on GO, RGO and Gr (Liu et al., 2009; Bautista-Toledo et al., 2005). Since the adsorption capacity of GO was increased for NaCl concentration of 1 mol/L, for the sake of comparison, all experiments were performed at this concentration of ionic strength (Fig. 2).

3.3. *Effect of contact time*

The effect of contact time on the adsorption of BPA by GO, RGO and Gr is presented in Fig. 3a. The adsorption achieved equilibrium at about 60 min for GO, suggested that GO showed very rapid adsorption. For RGO and Gr the adsorption increased rapidly in the first 5 min and equilibrium was reached at 30 min. After 60 min the observed plateau in Fig. 3a suggested the end of the process. This faster adsorption for RGO and Gr can be attributed to the single sheet structure of RGO and Gr that makes easier and more effective the BFA contact with the surface of RGO and Gr.

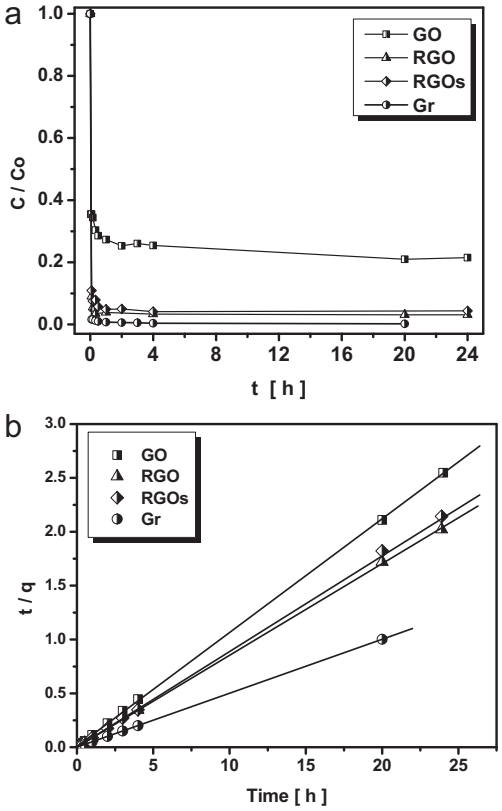

Fig. 3 – (a) Effect of contact time on the adsorption of BPA on GO, RGO RGOs and Gr. (b) Kinetic results for GO, RGO RGOs and Gr applied to the linear form of the pseudo-second-order model.

The experimental data were fitted to the pseudo-first-order and pseudo-second-order kinetic models applied to the linear form. The pseudo-second-order rate constant (k_2) and the amounts of BPA, adsorbed at equilibrium (q_e) were calculated from the intercept and slope of the plot of t/qt vs t according to Eq. (3) and the kinetic results applied to the linear form of the pseudo-second-order model are presented in Fig. 3b, while the relative kinetic parameters are shown in Table 1. The correlation coefficient R^2 value for the pseudo-second-order model was much higher than that of the pseudo-first-order model indicating that the pseudo-second-order kinetic model provided a better correlation in contrast to the pseudo-first-order model, that presented low correlation coefficient R^2 (data not presented) for the adsorption of BPA on GO, RGO and Gr, suggesting that BPA sorption onto these adsorbents is dependent on the amount of the solute adsorbed on the surface of adsorbent and the amount adsorbed at equilibrium (Ho, 2006; Sparks, 1986).

3.4. *Isotherms—Thermodynamics*

The effect of initial ion concentration on BFA adsorption on GO, RGO RGOs and Gr was examined and evaluated with the Langmuir and Freundlich isotherms. In Fig. 4 the aforementioned effect at 25 °C is presented for all sorbents for the sake of comparison while in Table 2 the regression parameters of the Langmuir and Freundlich models are presented. From the Table, comparing the R^2 it is concluded that the Langmuir model better describes the adsorption of BPA onto all adsorbents. It is also observed that Gr presented higher maximum adsorption capacity (Q_m) than RGO, RGOs and GO. Specifically,

Table 1 – Kinetic parameters for the adsorption of BPA on GO, RGO RGOs and Gr.

Adsorbent	Pseudo-second order			
	k_2 (g/mg/min)	q_e (mg/g)	h (mg/g/min)	R^2
GO	0.02	9.47	1.95	0.9999
RGO	0.07	11.75	9.80	0.9998
RGOs	0.14	11.27	18.06	0.9992
Gr	0.15	19.96	63.06	1

Table 2 – Equilibrium parameters for the adsorption of BPA at 25 °C onto GO, RGO, RGOs and Gr.

Samples	°C	Langmuir model			Freundlich model		
		Q_{max}	K_L	R^2	K_F	$1/n$	R^2
GO	25	17.27	0.1725	0.9314	5.0268	0.2992	0.7718
RGO	25	80.81	0.2872	0.9831	24.0324	0.3249	0.8739
RGOs	25	78.83	0.1651	0.9983	nd	nd	nd
Gr	25	94.06	0.5912	0.9909	32.1218	0.2870	0.9705

Table 3 – Q_{max} for BPA adsorption exhibited by sorbent materials in literature.

Adsorbent materials	Q_{max} (mg/g)	Reference
Activated carbon commercial	130	Bautista-Toledo et al. (2005)
(Sorbo-Norit, 3-A-7472)	9.1324	Zhou et al. (2016)
Reduced graphite oxide-magnetic nanoparticles (RGO-MNPs)	106.4	Zhang and Cheng (2014)
Magnetite (Fe_3O_4)	5.08	Li et al. (2015)
10% CNTs/Fe_3O_4	44.40	Li et al. (2015)
50% CNTs/Fe_3O_4	43.76	Li et al. (2015)
CNTs	46.18	Li et al. (2015)

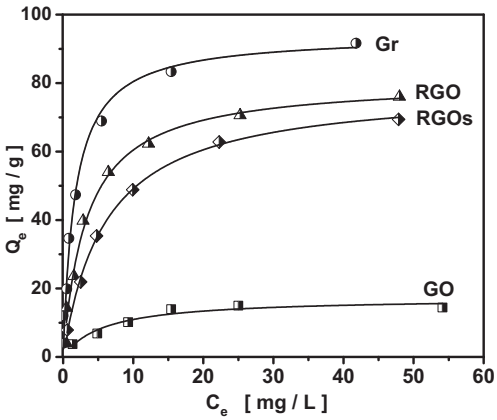

Fig. 4 – Effect of initial concentration on adsorption of BPA onto GO, RGO, RGOs and Gr, fitted to Langmuir and Freundlich isotherms.

GO presented Q_{max} of 17.27 mg/g, while RGO of 80.81 and Gr of 92.69 mg/g. These differences in Q_{max} can be attributed to the difference textural and mainly surface chemistry properties of the adsorbents as will be further discussed (Table 3).

Equilibrium experiments were also performed at 45 °C and 65 °C. The adsorption results expressed by the Freundlich and Langmuir models are presented in Fig. 5 and the regression parameters of the models are collected in Table 4.

Thermodynamic analysis was also done, based on the change of Gibbs free energy (ΔG°, kJ/mol), change of enthalpy (ΔH°, kJ/mol) and entropy change (ΔS°, kJ/mol K). These parameters calculated for the experiments performed at pH = 3 and at 25, 45 and 65 °C, are also presented in Table 4. The negative values of ΔG° showed the spontaneous adsorption of BA onto the under examination adsorbents and the thermodynamic feasibility of the adsorption. The decrease of the

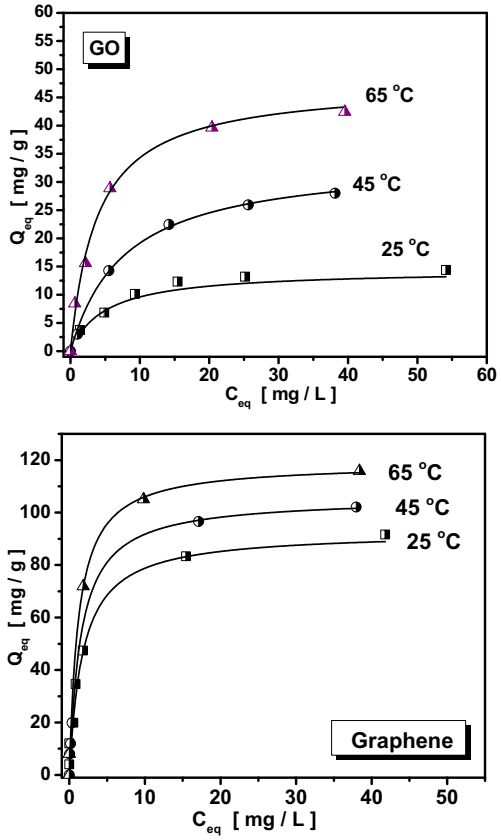

Fig. 5 – Effect of initial concentration and temperature (25, 45, 65 °C) on adsorption of BPA onto GO and Gr fitted to Langmuir and Freundlich isotherms.

Table 4 – Thermodynamic parameters for the adsorption of BPA on GO, RGO, RGOs and Gr.

Samples	T (°C)	Langmuir model			ΔG° (kJ/mol)	ΔH° (kJ/mol)	ΔS° (kJ/mol/K)
		Q_{max}	K_L	R^2			
GO	25	17.27	0.1725	0.9314	−2.574	44.936	0.159
	45	34.04	0.1287	0.9954	−6.045		
	65	47.51	0.2594	0.9884	−8.963		
Gr	25	94.06	0.5912	0.9909	−13.703	45.141	0.193
	45	104.98	0.6676	0.9933	−14.319		
	56	118.84	0.8266	0.9865	−21.456		

values of ΔG° with the increase of the temperature indicates that adsorption becomes more favorable at higher temperatures. The values of ΔG° also could indicate the nature of adsorption i.e. values at the range of 0 to −20 kJ/mol and −80 to −400 kJ/mol are indicative for physical or chemical adsorption, respectively. From the values of ΔG° estimated in this study it is concluded that the adsorption process is mainly physical in nature. The positive values of ΔH° indicated the endothermic nature of the process. These values were reduced with the increase of BPA concentration. The latter could be linked with the fact that in an endothermic process, the adsorbate had to displace more than one water molecule for their adsorption and this resulted in the endothermicity of the adsorption process; therefore ΔH° would be positive. Moreover, the values of ΔS° were found to be positive, which reflected the affinity of the adsorbent towards the adsorbate species. In addition, the positive value of ΔS° suggested increased randomness at the solid/solution interface with some structural changes in the adsorbate and adsorbent. The positive ΔS° value also corresponded to an increase in the degree of freedom of the adsorbed (Zhang et al., 2013).

3.5. *Desorption*

Desorption plays an important role for the selection of a sorbent material since the regeneration and the reuse of adsorbents as well as the recovery of the adsorbate is a crucial industrial demand. In order to remove the adsorbed BPA, the spent adsorbents firstly were treated with distilled water at different pH values, equilibrated for 24 h filtered and the filtrate was measured for the desorbed BPA. For GO the optimum pH for desorption found to be 10 as it is presented in Fig. 6a; at this pH value about 95% of BPA could be desorbed from the sorbent surface. The effect of pH on desorption was insufficient for RGO and Gr; the desorption percentages for these samples was less than 20% while the optimum pH for desorption found to be 10 for all samples, pH value that was the inverse than the optimum pH of adsorption, in which pH the bonds between BPA molecules and sorbents are weaken. The organic eluents achieved desorption of about 100% for the diethyl ether—methanol 9:1 mixture (Fig. 6b) and ethanol to present a 80% desorption of the BPA for GO and RGO. The desorption percentage of BPA followed the sequence: diethyl ether–methanol 9:1 > ethanol > acetonitrile > methanol for RGO while for GO acetonitrile and methanol did not achieve any desorption. In conclusion, the mixture diethyl ether-methanol proved to be the most suitable eluent.

3.6. *Sorbent characterization—Adsorption mechanism*

In order to explain the above adsorption results and the observed adsorption behavior of the sorbents, the surface

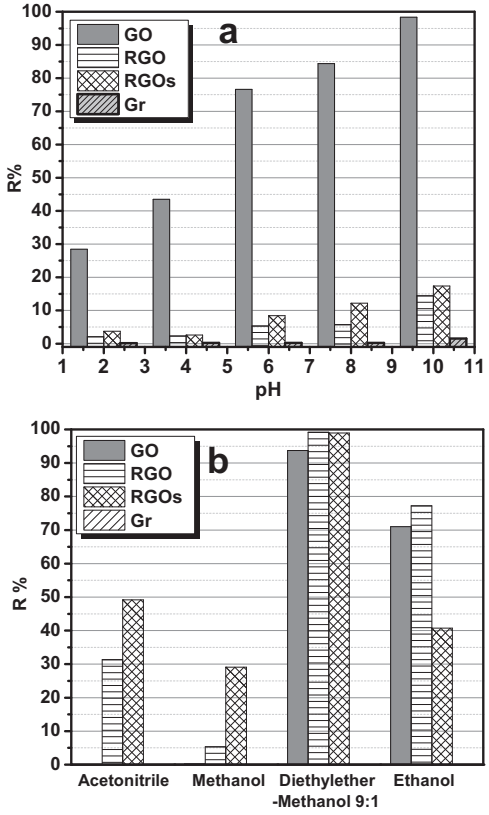

Fig. 6 – (a) Effect of pH on BPA desorption from GO, RGO, RGOs and Gr. (b) Effect of organic solvents on BPA desorption from GO, RGO, RGOs and Gr.

features of their initial and after BPA adsorption have to be analyzed in detail. Even though these initial materials have been previously discussed (Stobinsky et al., 2014a,b) the information about their porous structure and surface chemistry is crucial for the proper perspective on the adsorption/reactive adsorption mechanism of this endocrine disruptor.

3.6.1. *XRD measurements*

X-ray diffraction patterns of the materials measured in a range of 2θ from 5° to 50° are presented in Fig. 7 providing interesting information about their structure. Fig. 7 shows a relatively sharp (0 0 2) diffraction peak at 2θ = 9.98° for GO indicative of a well-defined layered structure and at 2θ = 24° for RGO and Gr, as well as diffraction peak at 2θ = 42° for GO and at 43° for RGO and Gr, indicating a short range order in stacked graphene layers. The corresponding interlayer spacing of GO as determined by Bragg's law was about 0.81 nm (Jeong et al., 2008).

As expected, after graphite oxidation the interlayer distance between the carbon layers, increased from 0.336 nm for graphite (Jeong et al., 2008) to 0.81 nm for graphite oxide that can be attributed to the amount of polar groups generated

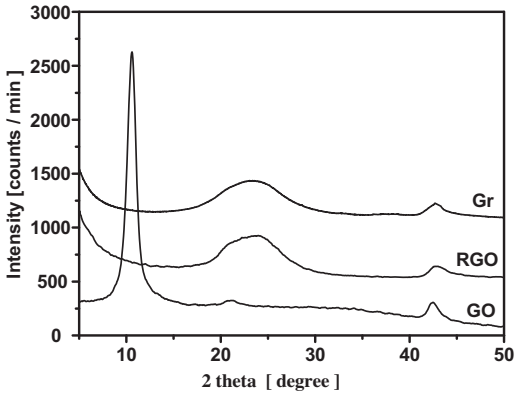

Fig. 7 – X-ray diffraction patterns of GO, RGO and Gr.

between the layers of graphite (Stobinsky et al., 2014a,b). To these groups the oxygen and carbon atoms are covalently bonded and as a result there is an increase in the graphite's crystal lattice length along axis *c*. Besides, the existence of polar groups causes a strong hydroscopicity of GO, and entrance of water molecules between the layers, hydrogen bonded with the oxygen atoms of the acidic groups, enlarging further the interlayer distance (Seredych et al., 2010).

The Scherrer equation was applied for estimating the average diameter of stacking layers, denoted as *D*. The GO consists of 8 graphene layers. After reduction (RGO and Gr samples) only the broad humps from the disordered carbon phase are seen as a result of the exfoliation of the GO structure. Calculation of the average size of the crystallite using the Sherrer's equation brings results about 1.34 nm for RGO and 1.21 for Gr. From that data and the d_{002} the number of layers was calculated and found that RGO consists of 3–4 layers and Gr of about 3 (Seredych et al., 2010). In the reduced graphite oxides the average number of layers decreases about 50% compared to the parent GO. This might be the apparent result of an increased heterogeneity of the materials since the observed peaks are broad (Stobinsky et al., 2014a,b).

3.6.2. *Surface properties-BET and SEM images*

An important parameter of adsorption performance is the porosity and nitrogen adsorption measurement is a useful mean for the characterization of porosity since it provides information about the textural characteristics and the surface area that is available to the adsorbate. N_2 adsorption-desorption isotherms for GO are presented in Fig. 8a. GO exhibited a type IV isotherm, as classified by IUPAC classification, with a hysteresis loop at the relative pressure range (P/P_o) of 0.45–1.00, suggesting this way mesoporosity (Foo and Hameed, 2011). GO exhibited a relatively low BET specific surface area (SSA) of 20.93 m^2/g due to the severe aggregation of GO sheets during desiccation (Seredych et al., 2010). The specific surface areas and the porosity parameters exhibited by the under examination adsorbents were calculated and presented in Table 5.

Reduction of GO caused an increase in the porosity as a result of exfoliation and rearrangement of layers (Stankovick et al., 2007). For Gr the volumes of pores were reduced may be due to the reactions of ammonia with surface groups and the deposition of new products inside the pore system.

Pore size distribution is also an important aspect of porous carbonaceous materials since it characterizes their structural heterogeneity. According to IUPAC classification, porous carbonaceous materials are classified into microporous (pore

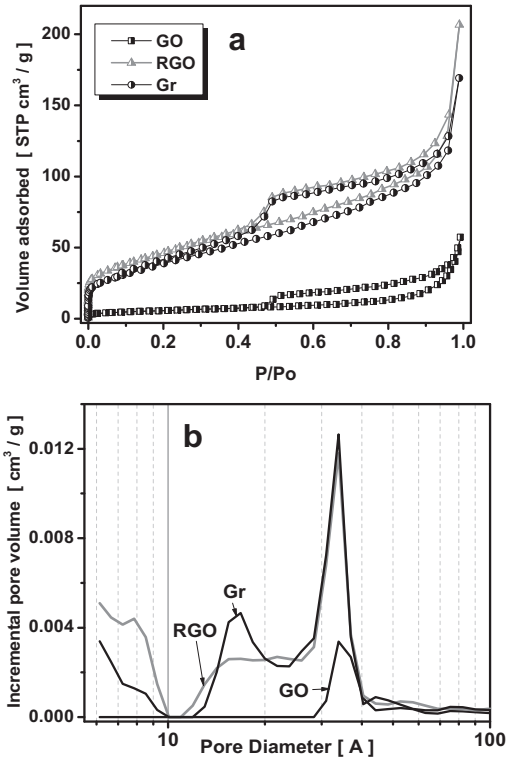

Fig. 8 – (a) N_2 adsorption isotherms for GO, RGO and Gr. (b) Pore size distribution (DFT) curves for GO, RGO and Gr.

size <2 nm), mesoporous (pore size = 2–50 nm) and macroporous (pore size >50 nm) (Foo and Hameed, 2011). The pore size distributions exhibited by GO, RGO and Gr, calculated by the density functional theory (DFT) method are presented in Fig. 8b. As appeared in this Figure, the width of the pores in all sorbents sheets found to be about 3.5 nm. Since the largest length of BPA molecule was 0.94 nm (Franz et al., 2000) the pore size of all adsorbents was sufficiently big for BPA molecules to access to the functional groups on the surface of these adsorbents that could be good candidates as adsorbents.

The changes in porosity are supported by SEM micrographs that are presented in Fig. 9. Reduction with hydrazine of GO increases the heterogeneity which results in a slight increase in the porosity. The SEM images showed that all three samples displayed typical rippled and crumpled surfaces indicative of graphene. The size of the GO nanosheets was large and the surfaces were relatively flat (Fig. 9c) compared with those of RGO and Gr. After reduction, the large GO nanosheets were divided into small fragments. The RGO and Gr nanosheets were slightly aggregated, having as result micro-pores created by the packed layers as was also shown by the nitrogen adsorption measurements.

3.7. *Surface chemistry-FTIR measurements*

The surface chemistry of sorbents plays an important role in their adsorption performance. Surface chemistry as well as the changes in the chemistry after BPA adsorption are reflected on proton binding curves and the results are presented in Fig. 10. After BPA adsorption the surface became much more basic for all sorbents due to deposition of BPA on their surface.

In order to understand the mechanism by which BFA was adsorbed on the under examination sorbents, FTIR spectra were obtained for the GO, RGO and Gr before and after BFA adsorption (Fig. 11). For GO, the peaks at 1060, 1240, 1380

Table 5 – Textural parameters calculated from nitrogen adsorption isotherms.

Adsorbent	SSA m^2/g	V_{tot} (cm^3/g)	V_{mic} (cm^3/g)	V_{DFT} (cm^3/g)	V_{mes} (cm^3/g)
GO	20.93	0.0886	0.0648	0.0581	0.0239
RGO	168.76	0.3197	0.2151	0.2082	0.1046
Gr	108.69	0.2617	0.1552	0.1861	0.1065

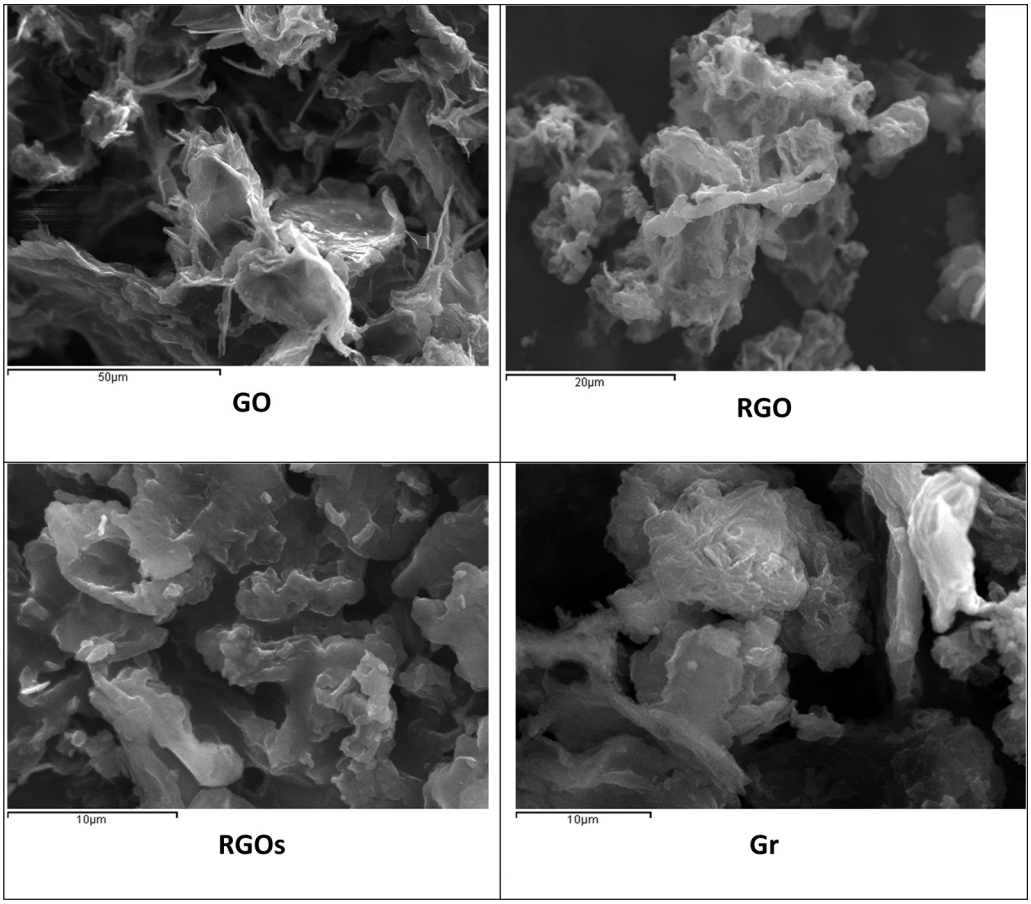

Fig. 9 – SEM images of GO, RGO, RGOs and Gr.

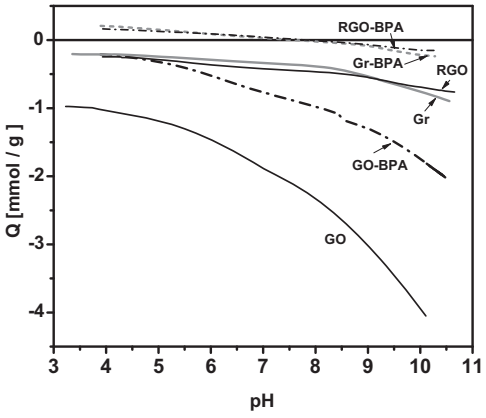

Fig. 10 – Proton binding curves for GO, RGO and Gr and their counterparts after BPA adsorption.

and 1730 cm^{-1} correspond to the stretching vibration of the C–O (alkoxy) C–O–C (epoxy) bonds O–C=O (carboxyl) and C=O respectively (Giannakoudakis et al., 2016; Socrates, 1994). The well visible vibration at 1240 cm^{-1} can be also related to S=O asymmetric stretching vibration in sulfones or sulfates. The band at 1625 cm^{-1} was indicative of C=C (C–C) skeletal contributed from the aromatic ring mode (Giannakoudakis and Bandosz, 2014; Dreyer et al., 2010) conjugated carbonyl and carboxylate groups due to the presence of graphene-like domain on the GO nanosheets, while in the range of higher wavenumbers three separate –OH modes can be identified with absorptions at 3610, 3420, and 3170 cm^{-1} (Seredych et al., 2010). They must represent the vibration of O–H in as isolated hydroxyl groups, intercalated H_2O, and –COH, respectively. Due to the abundant surface functional groups GO presented a higher hydrophilicity and a better water dispersibility.

For RGO and Gr it is evident that the peaks at 1730 cm^{-1} (C=O), approximately 1380 cm^{-1} (O=C–O), 1240 cm^{-1} (C–O–C) and approximately 1060 cm^{-1} (alkoxy C–O) were weaker or absent the intensity of the O–H bond at 3435 cm^{-1} was weaker compared with that of GO. These indicated that many oxygen-containing functional groups were removed via chemical reductions, making the surfaces of RGO and Gr highly hydrophobic. The peak at 1580 cm^{-1} were assigned to the C=C stretching vibration. This peak was presented as a complex band after hydrazine treatment that can be also attributed to amine/amide groups (Seredych et al., 2010). The C=O bond at 1730 cm^{-1} on RGO and Gr spectra was absent when compared with the spectrum of GO, indicating that functional groups containing a C=O bond could be altered or eliminated by hydrazine reduction and by the reactions of carboxylic

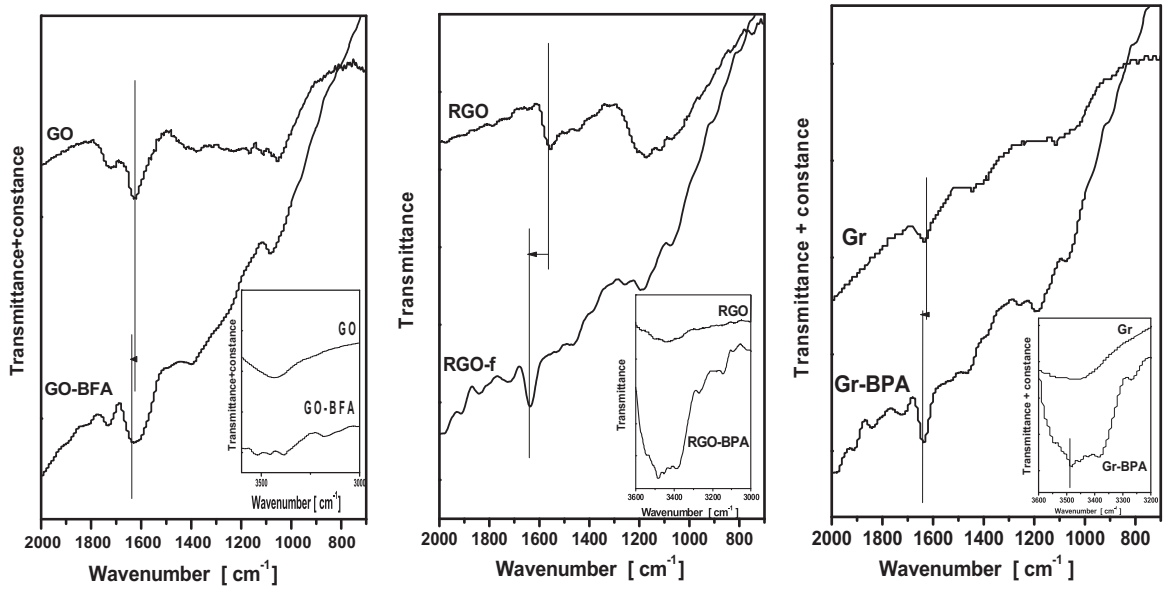

Fig. 11 – FTIR spectra of the studied samples before and after BFA adsorption.

groups with ammonia. Besides the decrease in the intensity of the 1730 cm^{-1} band a relative increase in the intensity of the band at 1630 cm^{-1} was noticed that can be indicative of amine formation via the reaction of NH_3 with epoxy groups and/or amides via the reaction of ammonia with carboxylic acids (Stankovick et al., 2007).

In the spectra of the BPA loaded samples the intensity of the band for the O—H group at 3481 cm^{-1} increased for the RGO and Gr (inset Figures in Fig. 11a–c) indicating that a certain number of BPA molecules had been adsorbed on the surface of these sorbents. This increase is more obvious for the RGO and Gr. During the reduction of GO, hydrazine hydrate reacts with epoxide groups leading to the formation amine/amide groups and/or of an aminoaziridine moieties (Dreyer et al., 2010; Zhang and Cheng, 2014) that could be ascribed to hydrogen bonding interactions with the O—H groups of BPA and these aminoaziridine moieties (Lin and Xing, 2008). Furthermore, the bands at 1160 cm^{-1}, that correspond to the O—H bend/stretch, shifted from 1160 to 1220 cm^{-1} in the spectra for the samples after BPA sorption, indicating interaction of these groups with the —OH groups of the BPA. In Fig. 11a–c it is also presented that the peak belonging to the skeletal vibration of aromatic C=C bonds after sorption shifted from 1610 to 1626 cm^{-1}, for all samples, indicating π–π interaction between the benzene rings of the sorbents and those of BPA. The adsorption of organic pollutants on graphene based materials could be attributed to π–π interactions of π electrons of these organic pollutants with the π electrons of the benzene rings of the graphene materials (Lin and Xing, 2008; Zhu and Pignatello, 2005). Thus, FTIR results suggest that BPA was adsorbed on GO, RGO and Gr surface and the mechanisms of its adsorption are the π–π interactions of π electrons of the benzene rings of BPA with the π electrons of benzene rings of these sorbents and hydrogen bonding between the —OH groups of BPA and the sorbents.

3.8. *Adsorption mechanism of graphene materials*

The adsorption affinities of BPA onto the three adsorbents followed the order of GO < RGO < Gr. There was not found any correlation between the specific surface areas (SSA) and the maximum capacity of the adsorption processes, since the SA of RGO (168.7 m^2/g) was approximately 8 times than that of GO (20.9 m^2/g) and 1.5 times that of Gr (108.7 m^2/g), while the adsorption capacity of RGO (Q_{max} = 80.81 mg/g) was approximately 5 times that of GO (Q_{max} = 17.27 mg/g) and less than that of Gr (94.06 mg/g). Considering the capacity per specific surface area of the sorbens (mg/m^2) it was found 0.8223 mg/m^2 for GO, 0.4788 mg/m^2 for RGO and 0.8653 mg/m^2 for Gr showing again no correlation between the maximum adsorption capacity and the capacity per surface area of the sorbents.

The adsorption mechanisms of aromatic organic molecules onto carbon and graphene based materials have commonly been interpreted with the π–π interaction, hydrophobic effect, H-bonding and electrostatic interaction (Wang et al., 2014; Xuebao, 2013; Xu et al., 2012). BPA has a low hydrophobicity (Foo and Hameed, 2011) thus, a hydrophobic effect does not dominate the adsorption of BPA onto graphene materials. Aromatic organic molecules are demonstrated to adsorb onto graphene nanosheets primarily through π–π interactions, so the elimination of oxygen-containing functional groups can significantly enhance the interaction between the π system of graphene and the π units of aromatic molecules (Zhang et al., 2013).

For RGO and Gr, the adsorption of BPA was nearly constant with increasing pH and reached a prominent adsorption minimum as the pH approached the pKa of BPA (9.34). This decrease can be attributed to the fact that the surface of RGO and Gr presented negatively charged surface as the pH approached the pKa of BPA (Fig. 1b), so, strong electronic repulsion between the negatively charged sorbents and dissociated BPA at this pH (pH = 10) suppressed the uptake of BPA. In contrast, the adsorption of BPA onto GO decreased with increasing pH (3 to 9). The presence of oxygen-containing functional groups on GO reduced the hydrophobicity (Wang et al., 2014), prohibited the aromatic adsorption sites on GO to be easily available in the aqueous solution for the π–π interaction, and made the surface charge more electronegative (i.e., more responsive to pH changes) (Lee et al., 2005). At low pH values, the surface of GO was electron depleted and could serve as a Lewis acid. Correspondingly, BPA could serve as a Lewis base, and thus, the adsorption of BPA onto GO was stronger at low pH values because of the more electron depleted GO (Zhu et al., 2004).

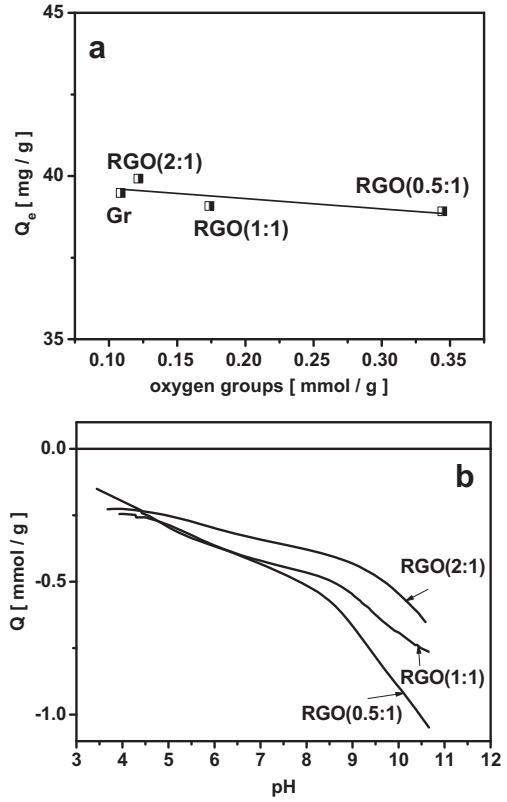

Fig. 12 – (a) Correlation between the oxygen surface groups and the adsorption capacity (b) potentiometric titration curves for the $RGO_{2:1}$, $RGO_{1:1}$ and $RGO_{0.5:1}$ samples.

From the above it was concluded that with the increase of the reduction degree of GO, the adsorption capacities of BPA increased. As discussed, the chemical reduction treatment removed most of the oxygen-containing functional groups on the surface of GO and introduced aminoaziridine moieties. Since it was found that the nitrogen-containing groups although contributed to adsorption through hydrogen-bonding interactions (G—NH_2···HO—R) could not be considered as a major influencing factor (Wang et al., 2014), the oxygen-containing functional groups decrease could be involved. In order to testify whether the eliminated after reduction oxygen-containing groups could contribute to the increased sorption, the adsorption capacities for BPA was evaluated at the same initial concentration of BPA, for the samples: $RGO_{0.5:1}$, $RGO_{1:1}$ and $RGO_{2:1}$ and Gr. The effect of the increase of the reduction degree of GO to oxygen-containing functional groups decrease and consequently to the decrease on the surface charge of the relative RGO prepared, was illustrated on the proton-binding curves of these samples after potentiometric titration results (Fig. 12b), where it is obvious that the more effective the reduction the less negative their surface charge. It was found that the adsorption capacities of these samples presented a linear correlation to the amount of their acidic groups and the less oxygen acidic groups were deposited on their surface, the greater adsorption capacity it was presented (Fig. 12a).

The results make obvious that graphene based materials have strong adsorption affinity for aromatic compounds due to the π-electron-rich property and can interact with aromatic compounds through the π-electron-coupling ability. The increase in the degree of GO reduction reduced the amount of oxygen-containing functional groups on the surface of RGO samples, leading to the increase of the π–π interaction between sorbent–adsorbate and to linearly increased adsorption capacity.

4. Conclusions

The adsorption of Bisphenol A, a non-polar organic, in aqueous solutions onto graphene based materials was examined. The adsorption isotherm constants were evaluated by using Langmuir and Freundlich isotherms and it is concluded that the Langmuir isotherm fitted better for all samples, indicating monolayer adsorption on a homogenous surface. The best adsorption capacities for GO, RGO and Gr were found to be 17.27 mg/g, 80.81 mg/g and 94.06 mg/g, respectively at 25 °C. The adsorption of Bisphenol A onto GO at a great extent and onto RGO and Gr at a smaller, was found to be dependent on the pH solution, initial BPA concentration, contact time and temperature with the maximum removal to be attained at pH 3. The thermodynamic parameters indicated a spontaneous and endothermic adsorption. The kinetic model analyses revealed that the experimental data were well fitted to the pseudo-second-order model. Desorption of BPA could be totally carried out using a diethyl ether-methanol 9:1 (v/v) mixture.

The adsorption of Bisphenol A, was found to be highly dependent by the oxygen-containing functional groups of graphene nanosheets. Interaction mechanisms, such as π-π, and *n–p* EDA interactions are involved in the adsorption processes. For a wide pH range, RGO and Gr showed sufficient adsorption capacities for BPA. By regulating the oxygen-containing functional groups on graphene nanosheets, graphene materials have great potential in pollution control applications.

References

Ahmaruzzaman, Md., 2008. Adsorption of phenolic compounds on low-cost adsorbents: a review. Adv. Colloid Interface Sci. 143, 48–67.

Asada, T., Oikawa, K., Kawata, K., Ishihara, S., Ivobe, T., Yamada, A., 2004. Study of removal effect of Bisphenol A and beta-estradiol by porous carbon. J. Health Sci. 50, 588–593.

Balandin, A.A., Ghosh, S., Bao, W., Calizo, I., Teweldebrhan, D., Miao, F., Lau, C.N., 2008. Superior thermal conductivity of single-layer graphene. Nano Lett. 8, 902–907.

Bautista-Toledo, I., Ferro-Garcia, M.A., Rivera-Utrilla, J., Moreno-Castilla, C., Vegas Fernandez, F.J., 2005. Bisphenol A removal from water by activated carbon. Effects of carbon characteristics and solution chemistry. Environ. Sci. Technol. 39, 6246–6250.

Bautista-Toledo, M.I., Rivera-Utrilla, J., Ocampo-Pérez, R., Carrasco-Marvn, F., Sanchez-Polo, M., 2014. Cooperative adsorption of bisphenol-A and chromium(III) ions from water on activated carbons prepared from olive-mill waste. Carbon 73, 338–350.

Belfroid, A., van Velzen, M., van der Horst, B., Vethaak, D., 2002. Occurrence of Bisphenol A in surface water and uptake in fish: evaluation of field measurements. Chemosphere 49, 97–103.

Blanchard, G., Maunaye, M., Martin, G., 1984. Removal of heavy metals from waters by means of natural zeolites. Water Res. 18, 1501–1507.

Chang, H.S., Choo, K.H., Lee, B., Choi, S.J., 2009. The methods of identification, analysis, and removal of endocrine disrupting compounds (EDCs) in water. J. Hazard. Mater. 172, 1–12.

Dikin, D.A., Stankovich, S., Zimney, E.J., Piner, R.D., Dommett, G.H.B., Evmenenko, G., Nguyen, S.T., Ruoff, R.S., 2007. Preparation and characterization of grapheme oxide paper. Nature 448, 457–460.

Dong, Y., Wu, D.Y., Chen, X.C., Lin, Y., 2010. Adsorption of Bisphenol A from water by surfactant-modified zeolite. J. Colloid Interface Sci. 348, 585–590.
Dreyer, D.R., Park, S., Bielawski, C.W., Ruoff, R.S., 2010. The chemistry of graphene oxide. Chem. Soc. Rev. 39, 228–240.
El-Naas, M.H., Al-Muhtaseb, S.A., Makhlouf, S., 2009. Biodegradation of phenol by *Pseudomonas putida* immobilized in polyvinyl alcohol (PVA) gel. J. Hazard. Mater. 164, 720–725.
Fan, L., Luo, C., Li, X., Lu, F., Qiu, H., Sun, M.J., 2012. Fabrication of novel magnetic chitosan grafted with graphene oxide o enhance adsorption properties of methylene blue. J. Hazard. Mater. 215–216, 272–279.
Foo, K.Y., Hameed, B.H., 2011. Preparation of activated carbon from date stones by microwave induced chemical activation: application for methylene blue adsorption. Chem. Eng. J. 170, 338–341.
Foo, K.Y., Hameed, B.H., 2012. Coconut husk derived activated carbon via microwave induced activation: effects of activation agents, preparation parameters and adsorption performance. Chem. Eng. J. 184, 57–65.
Franz, M., Arafat, H.A., Pinto, N.G., 2000. Effect of chemical surface heterogeneity on the adsorption mechanism of dissolved aromatics on activated carbon. Carbon 38, 1807–1819.
Freundlich, H., 1906. Uber dye adsorption in hosungen. Z. Phys. Chem. 57, 387–470.
Furhacker, M., Scharf, S., Weber, H., 2000. Bisphenol A: emissions from point sources. Chemosphere 41, 751–756.
Gao, Y., Li, Y., Zhang, L., Huang, H., Hu, J., Shah, S.M., Su, X., 2012. Adsorption and removal of tetracycline antibiotics from aqueous solution by graphene oxide. J. Colloid Interface Sci. 368, 540–546.
Giannakoudakis, D.A., Bandosz, T.J., 2014. Zinc (hydr)oxide/graphite oxide/AuNPs composites: role of surface features in H_2S reactive adsorption. J. Colloid Interface Sci. 436, 296.
Giannakoudakis, D.A., Mitchell, J.K., Bandosz, T.J., 2016. Reactive adsorption of mustard gas surrogate on zirconium (hydr)oxide/graphite oxide composites: the role of surface and chemical features. J. Mater. Chem., A 4, 1008.
Harikishore, D., Reddy, K., Lee, Seung-Mok, 2013. Application of magnetic chitosan composites for the removal of toxic metal and dyes from aqueous solutions. Adv. Colloid Interface Sci. 201–202, 68–93.
Ho, Y.S., 2006. Review of second-order models for adsorption systems. J. Hazard. Mater. 136, 681–689.
Hummers Jr., W.S., Offeman, R.E., 1958. Preparation of graphitic oxide. J. Am. Chem. Soc. 80, 1339.
Jeong, H.K., Noh, H.J., Kim, J.Y., Jin, M.H., Park, C.Y., Lee, Y.H., 2008. X-ray absorption spectroscopy of graphite oxide. EPL 82 (6), 67004.
Kang, J.H., Kondo, F., Katayama, Y., 2006. Human exposure to Bisphenol A. Toxicology 226, 79–89.
Kim, Y.H., Lee, B., Choo, K.H., Choi, S.J., 2011. Selective adsorption of Bisphenol A by organic-inorganic hybrid mesoporous silicas. Microporous Mesoporous Mater. 138, 184–190.
Kuo, C.Y., 2009. Comparison with as-grown and microwave modified carbon nanotubes to removal aqueous Bisphenol A. Desalination 249, 976–982.
Langmuir, I., 1918. The adsorption of gases on plane surface of glass, mica and platinum. J. Am. Chem. Soc. 40 (9), 1361–1403.
Lee, H.B., Peart, T.E., 2000. Bisphenol A contamination in Canadian municipal and industrial wastewater and sludge samples. Water Qual. Res. J. Canada 35, 283–298.
Lee, Y., Yoon, J., Gunten, U.V., 2005. Kinetics of the oxidation of phenols and phenolic endocrine disruptors during water treatment with ferrate(Fe(VI)). Environ. Sci. Technol. 39, 8978–8984.
Lee, C., Wei, X., Kysar, J.W., Hone, J., 2008. Measurement of the elastic properties and intrinsic strength of monolayer graphene. Science 321, 385–388.
Li, Y., Zhang, P., Du, Q., Peng, X., Liu, T., Wang, Z., Xia, Y., Zhang, W., Wang, K., Zhu, H., Wu, D., 2011. Adsorption of fluoride from aqueous solution by graphene. J. Colloid Interface Sci. 363, 348–354.
Li, S., Gong, Y., Yang, Y., He, C., Hu, L., Zhu, L., Sun, L., Shu, D., 2015. Recyclable CNTs/Fe_3O_4 magnetic nanocomposites as adsorbents to remove Bisphenol A from water and their regeneration. Chem. Eng. J. 260, 231–239.
Lin, D.H., Xing, B.S., 2008. Adsorption of phenolic compounds by carbon nanotubes: role of aromaticity and substitution of hydroxyl groups. Environ. Sci. Technol. 42 (19), 7254–7259.
Liu, G.F., Ma, J., Li, X.C., Qin, Q.D., 2009. Adsorption of Bisphenol A from aqueous solution onto activated carbons with different modification treatments. J. Hazard. Mater. 164, 1275–1280.
Meyer, J.C., Geim, A.K., Katsnelson, M.I., Novoselov, K.S., Booth, T.J., Roth, S., 2007. The structure of suspended graphene sheets. Nature 446, 60–63.
Mkhohan, K.A., Silicox, A.W., Stewart, D.A., Eda, G., 2009. Atomic and electronic structure of graphene oxide. Nano Lett. 9 (3), 1058–1063.
Pan, B., Lin, D.H., Mashayekhi, H., Xing, B.S., 2009. Adsorption and hysteresis of Bisphenol A and 17 alpha-ethinyl estradiol on carbon nanomaterials. Environ. Sci. Technol. 43, 5480–5485.
Seredych, M., Tamashausky, A.V., Bandosz, A.V., 2010. Graphite oxides obtained from porous graphite: the role of surface chemistry and texture in ammonia retention at ambient conditions. Adv. Funct. Mater. 20, 1670–1679.
Shniepp, H.C., Li, J.-L., Sai, H., Herrera-Alonso, M., 2006. Functionalized single graphene sheets derived from splitting graphite oxide. J. Phys. Chem., B 110, 8535–8539.
Socrates, G., 1994. Infrared Characteristic Group Frequencies, second ed. John Wiley & Sons, New York, NY.
Sparks, D.L., 1986. Kinetics of reaction in pure and mixed systems. In: Sparks, D.L. (Ed.), Soil Physical Chemistry. CRC Press, Boca Raton, FL (USA), pp. 63–145.
Stankovick, S., Dikin, D.A., Piner, R.D., Kohlhaas, K.A., Kleinhammes, A., Jia, Y.Y., 2007. Synthesis of graphene-based nanosheets via chemical reduction of exfoliated graphite oxide. Carbon 45 (7), 1558–1565.
Staples, C.A., Dorn, P.B., Klecka, G.M., O'Block, S.T., Harris, L.R., 1998. A review of the environmental fate, effects, and exposures of Bisphenol A. Chemosphere 36, 2149–2173.
Staples, C.A., Dorn, P., Klecka, G.M., O'Block, S.T., Branson, D.R., Harris, L.R., 2000. Bisphenol A concentrations in receiving waters near US manufacturing and processing facilities. Chemosphere 40, 521–525.
Stobinsky, L., Lesiak, B., Malolepszy, A., Mazurkiewicz, M., Mierzwa, B., Zemek, J., Jiricek, P., Bieloshapka, I., 2014a. Graphene oxide and reduced graphene oxide studied by the XRD, TEM and electron spectroscopy methods. J. Electron Spectrosc. Relat. Phenom. 195, 145–154.
Stobinsky, I., Lesiak, B., Malolepszy, A., Mazurkiewicz, M., Mierzwa, B., Zemek, J., Jiricek, P., Bieloshapka, I., 2014b. Graphene oxide and reduced graphene oxide studied by the XRD, TEM and electron spectroscopy methods. J. Electron Spectrosc. Relat. Phenom. 195, 145–154.
Stoller, M.D., Park, S., Zhu, Y., An, J., Ruoff, R.S., 2008. Graphene based ultracapacitors. Nano Lett. 8, 3498–3502.
Ternes, T.A., Stumpf, M., Mueller, J., Haberer, K., Wilken, R.D., Servos, M., 1999. Behavior and occurrence of estrogens in municipal sewage treatment plants—I. Investigations in Germany, Canada and Brazil. Sci. Total Environ. 225, 81–90.
Triantafyllidis, S.K., Deliyanni, A.E., 2014. Desulfurization of diesel fuels: adsorption of 4,6-DMDBT on different origin and surface chemistry nanoporous activated carbons. Chem. Eng. J. 236, 406–414.
Wang, J., Chen, B.B., 2015. Adsorption and coadsorption of organic pollutants and a heavy metal by grapheme oxide and reduced grapheme materials. Chem. Eng. J. 281, 379–388.
Wang, X., Zhi, L., Mullen, K., 2008. Transparent, conductive graphene electrodes for dye-sensitized solar cells. Nano Lett. 8, 323–327.

Wang, R., Ren, D., Xia, S., Zhang, Y., Zhao, J., 2009. Photocatalytic degradation of Bisphenol A (BPA) using immobilized TiO_2 and UV illumination in a horizontal circulating bed photocatalytic reactor (HCBPR). J. Hazard. Mater. 169, 926–932.

Wang, Xiaobo, Huang, Shuangshuang, Zhu, Lihua, Tian, Xiaolong, Li, Shenhui, Tang, Heqing, 2014. Correlation between the adsorption ability and reduction degree of graphene oxide and tuning of adsorption of phenolic compounds. Carbon 69, 101–112.

Xuebao, W.H., 2013. Elimination of Bisphenol A from water via graphene oxide adsorption. Acta Phys. Chim. Sin. 29 (4), 829–836.

Xu, J., Wang, L., Zhu, Y.F., 2012. Decontamination of Bisphenol A from aqueous solution by graphene adsorption. Langmuir 28 (22), 8418–8425.

Yang, S.T., Chang, Y.L., Wang, H.F., Liu, G.B., Chen, S., Wang, Y.W., Liu, Y.F., Cao, A.N.J., 2010. Folding/aggregation of grapheme oxide and its application in Cu^{2+} removal. Colloid Interface Sci. 351, 122.

Zhang, Y., Cheng, Y., 2014. Recyclable removal of Bisphenol A from aqueous solution by reduced graphene oxide-magnetic nanoparticles: adsorption and desorption. J. Colloid Interface Sci. 421, 85–92.

Zhang, Y., Causserand, C., Aimar, P., Cravedi, J.P., 2006. Removal of Bisphenol A by a nanofiltration membrane in view of drinking water production. Water Res. 40, 3793–3799.

Zhang, N., Qiu, H., Si, Y., Wang, W., Gao, J., 2011a. Fabrication of highly porous biodegradable monoliths strengthened by grapheme oxide and their adsorption of metal ions. Carbon 49, 827.

Zhang, W., Zhou, C., Zhou, W., Lei, A., Zhang, Q., Wan, Q., Zou, B., 2011b. Fast and considerable adsorption of methylene blue dye onto graphene oxide. Bull. Environ. Contam. Toxicol. 87, 86–90.

Zhang, W., Zhou, C., Zhou, W., Lei, A., Zhang, Q., Wan, Q., Zou, B., 2011c. Fast and considerable adsorption of methylene blue dye ono graphene oxide. Bull. Environ. Contam. Toxicol. 87, 86–90.

Zhang, Y., Tang, Y., Li, S., Yu, S., 2013. Sorption and removal of tetrabromobisphenol A from solution by graphene oxide. Chem. Eng. J. 222, 94–100.

Zhou, Q., Wang, Y., Xiao, J., Fan, H., 2016. Adsorption and removal of Bisphenol A, α-naphthol and β-naphthol from aqueous solution by Fe_3O_4@polyaniline core-shell nanomaterials. Synth. Met. 212, 113–122.

Zhu, D.Q., Pignatello, J.J., 2005. Characterization of aromatic compound sorptive interactions with black carbon (charcoal) assisted by graphite as a model. Environ. Sci. Technol. 39 (7), 2033–2041.

Zhu, D.Q., Hyun, S., Pignatello, J.J., Lee, L.S., 2004. Evidence for *p–p* electron donor–acceptor interactions between p-donor aromatic compounds and p-acceptor sites in soil organic matter through pH effects on sorption. Environ. Sci. Technol. 38, 4361–4368.